SAND2015-9121C

A Comparison of Reduced Order Modeling Techniques Used in Dynamic Substructuring

Dan Roettgen, Benjamin Seegar, Wei Che Tai, Seunghun Baek, Tilán Dossogne, Matthew Allen, Robert Kuether, Matthew R. W. Brake, Randall Mayes

ABSTRACT

Experimental dynamic substructuring is a means whereby a mathematical model for a substructure can be obtained experimentally and then coupled to a model for the rest of the assembly to predict the response. Recently, various methods have been proposed that use a transmission simulator to overcome sensitivity to measurement errors and to exercise the interface between the substructures; including the Craig-Bampton, Dual Craig-Bampton, and Craig-Mayes methods. This work compares the advantages and disadvantages of these reduced order modeling strategies for two dynamic substructuring problems. The methods are first used on an analytical beam model to validate the methodologies. Then they are used to obtain an experimental model for structure consisting of a cylinder with several components inside connected to the outside case by foam with uncertain properties. This represents an exceedingly difficult structure to model and so experimental substructuring could be an attractive way to obtain a model of the system.

Keywords Reduced order modelling, dynamic substructuring, Craig-Bampton, Craig-Mayes, Craig-Chang

Sandia National Laboratories is a multi-program laboratory managed and operated by Sandia Corporation, a wholly owned subsidiary of Lockheed Martin Corporation, for the U.S. Department of Energy's National Nuclear Security Administration under contract DE-AC04-94AL85000.

1 INTRODUCTION AND MOTIVATION

Experimental-analytical substructuring allows one to predict the dynamic response of an assembly by coupling substructures derived from experiments hardware with a finite element model representing the rest of the assembly. There are numerous applications of experimental analytical substructuring, but in particular this is useful when one has a subcomponent of a system that is difficult to model. This work looks at dynamic substructuring and the effects of using different reduced order models when completing the substructuring process by looking at two problems. First, a simple system is investigated using two beams connected by means of a transmission simulator. With this simple system, multiple dynamic substructuring and model reduction techniques are considered including the traditional transmission simulator [1−3], Craig-Bampton subcomponent assembly [4], Craig-Chang subcomponent assembly [4], and Craig-Mayes subcomponent assembly [5]. The second system consists of a beam attached to a plate on one end of a cylinder that encases a pressed foam and metal assembly. This second example uses actual experimental measurements while the beam example is purley a numerical demonstration. By using a finite element model of the beam-plate-can assembly, an experimental model of the dynamics for the internal foam system can be described using dynamic substructuring. This is investigated using the traditional transmission simulator and Craig-Mayes techniques.

The paper is organized as follows; Section 2 provides a high level look at a few of the model reduction and dynamic substructuring forms used in this work. In Sections 3 and 4 this theory is put to use with a simple beam substructuring system and the beam-plate-can system, respectively.

2 THEORY

2.1 Transmission Simulator

The transmission simulator is a useful tool in experimental analytical substructuring as described in [1−3] and is briefly described in this section. A key advantadge of this method is that the transmission simulator works to mass-load the interface and improve the modal basis of the subsystem. To complete the transmission simulator method, one takes experimental data on the substructure of interest, denoted subsystem *C*. Then a negative form of the subsystem *A*, the transmission simulator, is coupled to the system. Finally, the actual substructure of interest which can be modeled with a finite element program, denoted subsystem *D*, is coupled into the system. See Fig. 1.

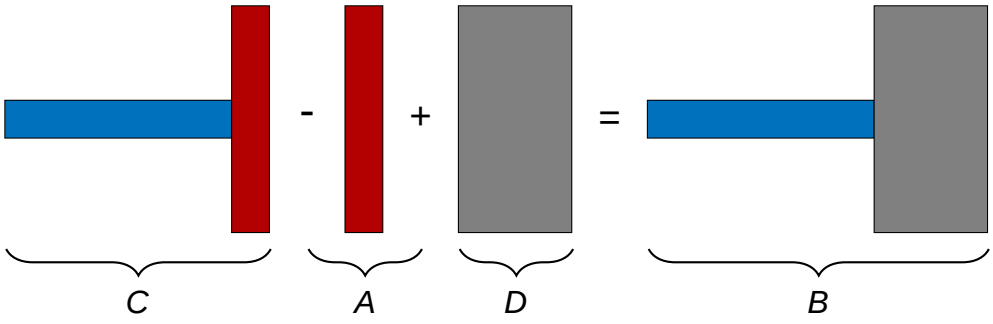

$$C - A + D = B$$

Figure 1: Transmission Simulator Diagram

Mathematically, to complete this substructuring the equations of motion of the experimental and analytical component are first converted into modal coordinates.

$$\begin{bmatrix} \mathbf{I}_C & 0 & 0 \\ 0 & \mathbf{I}_D & 0 \\ 0 & 0 & -\mathbf{I}_A \end{bmatrix} \begin{Bmatrix} \ddot{q}_C \\ \ddot{q}_D \\ \ddot{q}_A \end{Bmatrix} + \begin{bmatrix} \omega_C^2 & 0 & 0 \\ 0 & \omega_D^2 & 0 \\ 0 & 0 & -\omega_A^2 \end{bmatrix} \begin{Bmatrix} q_C \\ q_D \\ q_A \end{Bmatrix} = \begin{Bmatrix} \mathbf{\Phi}_C^T F_C \\ \mathbf{\Phi}_D^T F_D \\ \mathbf{\Phi}_A^T F_A \end{Bmatrix} \tag{1}$$

The physical constraints can be defined by equating the motion of each subsystem with that of the transmission simulator and then transformed into modal coordinates. This equation only applies to the subset of degrees of freedom which act to connect the transmission simulator between substructures.

$$\begin{bmatrix} \mathbf{I} & 0 & -\mathbf{I} \\ 0 & \mathbf{I} & -\mathbf{I} \end{bmatrix} \begin{Bmatrix} x_C \\ x_D \\ x_A \end{Bmatrix} = \begin{Bmatrix} 0 \\ 0 \\ 0 \end{Bmatrix} \tag{2}$$

$$\begin{bmatrix} \mathbf{\Phi}_C & 0 & -\mathbf{\Phi}_A \\ 0 & \mathbf{\Phi}_D & -\mathbf{\Phi}_A \end{bmatrix} \begin{Bmatrix} q_C \\ q_D \\ q_A \end{Bmatrix} = \begin{Bmatrix} 0 \\ 0 \\ 0 \end{Bmatrix} \tag{3}$$

In order to take advantage of the transmission simulator method, the constraints are now pre-multiplied by the pseudo-inverse of the transmission simulator mode shapes partitioned to the constraint degrees of freedom. This forces the projection of modal degrees of freedom q_A onto q_C.

$$\begin{bmatrix} \mathbf{\Phi}_A^\dagger & 0 \\ 0 & \mathbf{\Phi}_A^\dagger \end{bmatrix} \begin{bmatrix} \mathbf{\Phi}_C & 0 & -\mathbf{\Phi}_A \\ 0 & \mathbf{\Phi}_D & -\mathbf{\Phi}_A \end{bmatrix} \begin{Bmatrix} q_C \\ q_D \\ q_A \end{Bmatrix} = \begin{Bmatrix} 0 \\ 0 \\ 0 \end{Bmatrix} \tag{4}$$

The two leading matrices can now be collected to form a single matrix, **B**, that contains the constraints for the modal degrees of freedom.

$$\mathbf{B}\left\{\begin{array}{c} q_C \\ q_D \\ q_A \end{array}\right\} = \left\{\begin{array}{c} 0 \\ 0 \\ 0 \end{array}\right\} \tag{5}$$

These constrained modal degrees of freedom can be transformed by some matrix, **L**, into a set of unconstrained generalized coordinates. In order to avoid a trivial solution, **L** must reside in the null space of **B**.

$$\begin{aligned} \{q\} &= \mathbf{L}\{q_g\} & (6) \\ \mathbf{BL}\{q_g\} &= \mathbf{0} & (7) \end{aligned}$$

This transformation matrix, **L**, is then used in Eq. (1), which is also pre-multiplied by $\mathbf{L}^T$ resulting in the coupled equations of motion for the system. The modal properties for this system can then be found as the modal properties for the new analytically assembled system. A final transform can then used to bring the solution for the modal degrees of freedom back into the physical domain.

$$\mathbf{x} = \left[\begin{array}{ccc} \mathbf{\Phi}_C & 0 & 0 \\ 0 & \mathbf{\Phi}_D & 0 \\ 0 & 0 & \mathbf{\Phi}_A \end{array}\right] \mathbf{L}\{q_g\} \tag{8}$$

This is the basis of the transmission simulator method. In this work we will look at two main types of model reduction techniques. First, those involving fixed interface modes such as the Craig-Bampton formulation, and then those involving the free-interface modes such as the Craig-Chang formulation.

2.2 Craig-Bampton

In order to take a system of equations from the physical domain into a Craig-Bampton form, a few steps are involved. First, the degrees of freedom are partitioned into two sets; the boundary set (the *b*-set), where this substructure will eventually be interfaced with another piece, and the interior set (the *i*-set) which are the remaining degrees of freedom.

$$\begin{aligned} \mathbf{x} &= \left\{\begin{array}{c} \mathbf{x}_i \\ \mathbf{x}_b \end{array}\right\} & (9) \\ \mathbf{M} &= \left[\begin{array}{cc} \mathbf{M}_{ii} & \mathbf{M}_{ib} \\ \mathbf{M}_{bi} & \mathbf{M}_{bb} \end{array}\right] & (10) \\ \mathbf{K} &= \left[\begin{array}{cc} \mathbf{K}_{ii} & \mathbf{K}_{ib} \\ \mathbf{K}_{bi} & \mathbf{K}_{bb} \end{array}\right] & (11) \end{aligned}$$

The physical coordinates can then be transformed into Craig-Bampton coordinates using the transformation.

$$\mathbf{x} = \left\{\begin{array}{c} \mathbf{x}_i \\ \mathbf{x}_b \end{array}\right\} = \left[\begin{array}{cc} \mathbf{\Phi}_{ik} & \mathbf{\Psi}_{ib} \\ 0 & \mathbf{I}_{bb} \end{array}\right] \left\{\begin{array}{c} \mathbf{q}_k \\ \mathbf{x}_b \end{array}\right\} = \mathbf{T_{CB}} \left\{\begin{array}{c} \mathbf{q}_k \\ \mathbf{x}_b \end{array}\right\} \tag{12}$$

In the transformation matrix the first column partition are the fixed-interface modes. These can be described as the interior degree of freedom motion when the interface is fixed (or constrained in all interface degrees of freedom). The number of kept fixed-interface modes can be reduced to *k* in order to decrease the total number of degrees of freedom. The second column partition represents the constraint modes. These describe the motion of the system when each boundary degree of freedom is given a unit displacement while holding the other boundary degrees of freedom fixed. $\mathbf{q}_k$ is a set of displacements corresponding to the fixed-interface motion and $\mathbf{u}_b$ is preserved from the original equation of motion as the boundary physical degrees of freedom.

This transformation matrix can be used to transform the subcomponent mass and stiffness matrices into their Craig-Bampton formulations.

$$\mathbf{M_{CB}} = \mathbf{T_{CB}^T M T_{CB}} = \begin{bmatrix} \mathbf{I} & \mathbf{M}_{kb} \\ \mathbf{M}_{bk} & \hat{\mathbf{M}}_{bb} \end{bmatrix} \tag{13}$$

$$\mathbf{K_{CB}} = \mathbf{T_{CB}^T K T_{CB}} = \begin{bmatrix} \omega_k^2 & 0 \\ 0 & \hat{\mathbf{K}}_{bb} \end{bmatrix} \tag{14}$$

Assembly of two Craig-Bampton matrices can then be completed by simply writing the constraints equation coupling the boundary degrees of freedom between the two subsystems.[4] With this constraint equation, a transformation matrix can be defined in order to couple the systems. When in the Craig-Bampton form, the interface degrees of freedom are preserved and the number of fixed-interface modes can be reduced. It is not possible to measure the fixed interface modes experimentally but this reduction can be used in an analytically model. The Craig-Mayes method proposes a way to estimate these fixed interface modes from the free modes of **C**.

2.3 Craig-Mayes

The Craig-Mayes formulation [5] is a method to generate a Craig-Bampton representation for the experimental side of the substructure. The resulting form resembles the dynamics of subsystem *C* (the experiment) minus subsystem *A* (the transmission simulator). The Craig-Mayes method is a proposed method to create a Craig-Bampton like structure with experimentally measured results using the free modes of the transmission simulator. To begin the experimental data from subsystem *C* can be written in modal coordinates.

$$\left[\omega_n^2 - \omega^2 \mathbf{I}\right] \bar{\mathbf{q}} = 0 \tag{15}$$

One must assume that a transformation matrix, **T**, exists that would bring the experimental modal results of *C* into a Craig-Bampton like form

$$\bar{\mathbf{q}} = \mathbf{T} \left\{ \begin{array}{c} \bar{\mathbf{p}} \\ \bar{\mathbf{s}} \end{array} \right\} \tag{16}$$

where $\bar{\mathbf{q}}$ represents the experimentally derived modal degrees of freedom, $\bar{\mathbf{p}}$ represents the fixed-interface modal coordinates, or motion when the boundary is fixed, and $\bar{\mathbf{s}}$ are coordinates that describe the motion of the TS. For this Craig-Bampton like formulation the transmission simulator degrees of freedom are considered the boundary.

The fixed-interface modal coordinates are found by fixing the boundary degrees of freedom, where $\mathbf{\Psi}_b$ represents the free modes of the transmission simulator and $\mathbf{\Phi}_b$ represents the experimental derived modes both partitioned to the boundary (TS) degrees of freedom.

$$\mathbf{\Psi}_b^\dagger \mathbf{\Phi}_b \bar{\mathbf{q}} = 0 \tag{17}$$

The modal degrees of freedom can now be replaced by a new set of coordinates, $\bar{\eta}$, which satisfy the constraints by using,

$$\mathbf{\Psi}_b^\dagger \mathbf{\Phi}_b \mathbf{L}_{fix} \bar{\eta} = 0 \tag{18}$$

where, $\mathbf{L}_{fix}$ must reside in the null space of $\mathbf{\Psi}_b^\dagger \mathbf{\Phi}_b$. $\mathbf{L}_{fix}$ can then be used to transform the modal representation from Eq. (15). This transformed equation can be solved for the eigen vectors $\mathbf{\Gamma}$ which uncouple the fixed interface modal degrees of freedom, $\bar{\mathbf{p}}$.

$$\bar{\mathbf{q}} = \mathbf{L}_{fix} \mathbf{\Gamma} \bar{\mathbf{p}} \tag{19}$$

This solves the partition of the transformation matrix related to the fixed interface modal amplitude, $\bar{\mathbf{p}}$, from Eq. (16). The partition

associated with the boundary degrees of freedom, $\bar{\mathbf{s}}$, is found by setting the motion of the TS in the experimental system equal to the free modal motion of the TS.

$$\mathbf{\Phi}_b \bar{\mathbf{q}} = \mathbf{\Psi}_b \bar{\mathbf{s}} \tag{20}$$

The transformation matrix can now be defined as shown in the equation below.

$$\mathbf{T} = \begin{bmatrix} \mathbf{L}_{fix}\mathbf{\Gamma} & \mathbf{\Phi}_b^{\dagger}\mathbf{\Psi}_b \end{bmatrix} \tag{21}$$

Pre and post multiplying by $\mathbf{T}^T$ and $\mathbf{T}$ respectively results in a new set of equations of motion in terms of $\bar{\mathbf{p}}$ and $\bar{\mathbf{s}}$ coordinates.

$$\left[\begin{bmatrix} \omega_{fix}^2 & \mathbf{K}_{ps} \\ \mathbf{K}_{sp} & \mathbf{K}_{ss} \end{bmatrix} - \omega^2 \begin{bmatrix} \mathbf{I} & \mathbf{M}_{ps} \\ \mathbf{M}_{sp} & \mathbf{M}_{ss} \end{bmatrix} \right] \begin{Bmatrix} \bar{\mathbf{p}} \\ \bar{\mathbf{s}} \end{Bmatrix} = 0 \tag{22}$$

To remove the mass and stiffness of the transmission simulator, the terms are simply subtracted from the lower right partitions of the new equations of motion which pertains to the transmission simulator motion. This is done using the free modes of the transmission simulator as shown in Eq. (23).

$$\left[\begin{bmatrix} \omega_{fix}^2 & \mathbf{K}_{ps} \\ \mathbf{K}_{sp} & \mathbf{K}_{ss} - \omega_{\mathbf{TS}}^2 \end{bmatrix} - \omega^2 \begin{bmatrix} \mathbf{I} & \mathbf{M}_{ps} \\ \mathbf{M}_{sp} & \mathbf{M}_{ss} - \mathbf{I} \end{bmatrix} \right] \begin{Bmatrix} \bar{\mathbf{p}} \\ \bar{\mathbf{s}} \end{Bmatrix} = 0 \tag{23}$$

The coordinates, $\bar{\mathbf{s}}$, which are the amplitudes of a set of shapes that span the motion of the interface degrees of freedom, can be readily related to the interface motion $\mathbf{x}_b$ and thus when the substructuring model is written in this Craig-Mayes it is easily coupled with a finite element model of subsystem *D*.

2.4 Craig-Chang Reduction Method

While the Craig-Bampton method utilizes fixed-interface modes, there exists a family of model reduction techniques relying on a basis of free-interface modes. This basis must also include interface attachment modes in order to meet static completeness and rigid-body modes if the system possesses rigid-body degrees of freedom.

One of those techniques is the so-called Craig-Chang reduction method [4]. Physical coordinates are transformed into Craig-Chang coordinates by means of a transformation matrix combining rigid-body modes $\mathbf{\Psi}_r$, a set of kept free-interface normal modes $\mathbf{\Phi}_k$ and inertia-relief residual-flexibility attachment modes $\mathbf{\Psi}_d$. Using the same partition between internal (i) and boundary (b) degrees of freedom as before, the transformation can be written as follows.

$$\mathbf{x} = \begin{Bmatrix} \mathbf{x}_i \\ \mathbf{x}_b \end{Bmatrix} = \begin{bmatrix} \mathbf{\Psi}_{ir} & \mathbf{\Phi}_{ik} & \mathbf{\Psi}_{id} \\ \mathbf{\Psi}_{br} & \mathbf{\Phi}_{bk} & \mathbf{\Psi}_{bd} \end{bmatrix} \begin{Bmatrix} \mathbf{q}_r \\ \mathbf{q}_k \\ \mathbf{q}_d \end{Bmatrix} = \mathbf{T}_{\mathbf{CC}} \begin{Bmatrix} \mathbf{q}_r \\ \mathbf{q}_k \\ \mathbf{q}_d \end{Bmatrix} \tag{24}$$

The transformation matrix $\mathbf{T}_{\mathbf{CC}}$ is thus applied to mass and stiffness matrices of the component to reduce them into their Craig-Chang formulations as described in Eq. (25) and Eq. (26).

$$\mathbf{M}_{\mathbf{CC}} = \mathbf{T}_{\mathbf{CC}}^T \mathbf{M} \mathbf{T}_{\mathbf{CC}} = \begin{bmatrix} \mathbf{I}_r & 0 & 0 \\ 0 & \mathbf{I}_k & 0 \\ 0 & 0 & \hat{\mathbf{M}}_{dd} \end{bmatrix} \tag{25}$$

$$\mathbf{K}_{\mathbf{CC}} = \mathbf{T}_{\mathbf{CC}}^T \mathbf{K} \mathbf{T}_{\mathbf{CC}} = \begin{bmatrix} 0 & 0 & 0 \\ 0 & \omega_k^2 & 0 \\ 0 & 0 & \hat{\mathbf{K}}_{dd} \end{bmatrix} \tag{26}$$

Where $\hat{\mathbf{M}}_{dd} = \mathbf{\Psi}_d \mathbf{M} \mathbf{\Psi}_d$ and $\hat{\mathbf{K}}_{dd} = \mathbf{\Psi}_d \mathbf{K} \mathbf{\Psi}_d = \mathbf{\Psi}_{bd}$. Contrary to Craig-Bampton method, the interface degrees of freedom

are not preserved. Therefore, the assembly process of two components, one reduced using Craig-Bampton and the other by Craig-Chang, requires a constraint matrix **S** that is not simply boolean. Its expression is given by Eq. (28).

$$\left\{ \begin{array}{c} \mathbf{q}_d^{(\mathbf{CC})} \\ \mathbf{q}_r^{(\mathbf{CC})} \\ \mathbf{q}_{k_1}^{(\mathbf{CC})} \\ \hline \mathbf{q}_{k_2}^{(\mathbf{CB})} \\ \mathbf{u}_b^{(\mathbf{CB})} \end{array} \right\} = \mathbf{S} \left\{ \begin{array}{c} \mathbf{q}_r^{(\mathbf{CC})} \\ \mathbf{q}_{k_1}^{(\mathbf{CC})} \\ \hline \mathbf{q}_{k_2}^{(\mathbf{CB})} \\ \mathbf{u}_b^{(\mathbf{CB})} \end{array} \right\} \tag{27}$$

$$\mathbf{S} = \left[\begin{array}{cccc} -\left(\mathbf{\Psi}_{bd}^{(\mathbf{CC})}\right)^{\dagger} \mathbf{\Psi}_{br}^{(\mathbf{CC})} & -\left(\mathbf{\Psi}_{bd}^{(\mathbf{CC})}\right)^{\dagger} \mathbf{\Phi}_{bk_1}^{(\mathbf{CC})} & \mathbf{0}_{bk_2}^{(\mathbf{CB})} & -\left(\mathbf{\Psi}_{bd}^{(\mathbf{CC})}\right)^{\dagger} \\ & \mathbf{I}_{(r+k_1+k_2+b)} & & \end{array} \right] \tag{28}$$

Mass and stiffness matrices of the assembled system are then calculated by pre- and post-multiplying the associated matrices of the two components by the constraint matrix.

$$\mathbf{M}_{\mathbf{CC+CB}} = \mathbf{S}^T \left[\begin{array}{cc} \mathbf{M}_{\mathbf{CC}} & 0 \\ 0 & \mathbf{M}_{\mathbf{CB}} \end{array} \right] \mathbf{S} \tag{29}$$

$$\mathbf{K}_{\mathbf{CC+CB}} = \mathbf{S}^T \left[\begin{array}{cc} \mathbf{K}_{\mathbf{CC}} & 0 \\ 0 & \mathbf{K}_{\mathbf{CB}} \end{array} \right] \mathbf{S} \tag{30}$$

As the constraint matrix is obtained by enforcing the compatibility condition between boundary displacements of the two components, the assembly process is hence considered as a *primal* assembly. Another method based on free-interface normal modes but using a *dual* assembly is the so-called dual Craig-Bampton method [4], which is described below.

A few complications arise when using the Craig-Chang formulation with experimental measurements for substructure **C**. It requires the measurement of the free interface modes which is simple. It also requires the rigid body modes to be measured or obtained from a finite element model. In addition, all of these modes would need to be measured at the interface degrees of freedom. These can be obtained from an input that excites all of the modes of interest. Finally one must determine a method to measure the residual flexibility at the interface. This requires an input and output at each interface degree of freedom which is not very feasible in an experimental set-up.

2.5 Dual Craig-Bampton Method

Dual assembly of components uses interface forces and consequently, compatibility at boundaries is weakly enforced in comparison with primal assembly. Equations of motion of each subcomponent can be expressed with the explicit formulation of those interface forces by means of Lagrange multipliers λ and constraint matrix **C**.

$$\left[\begin{array}{cc} \mathbf{M} & 0 \\ 0 & 0 \end{array} \right] \left\{ \begin{array}{c} \ddot{\mathbf{x}} \\ \lambda \end{array} \right\} + \left[\begin{array}{cc} \mathbf{K} & -\mathbf{C}^T \\ -\mathbf{C} & 0 \end{array} \right] \left\{ \begin{array}{c} \mathbf{x} \\ \lambda \end{array} \right\} = \left\{ \begin{array}{c} F \\ 0 \end{array} \right\} \tag{31}$$

Similarly to Craig-Chang techniques, the dual Craig-Bampton is based on free-interface normal modes and residual-flexibility attachment modes. Therefore, the displacement of each subsystem can be expressed as follows.

$$\mathbf{x} = \mathbf{\Psi}_r \mathbf{q}_r + \mathbf{\Phi}_k \mathbf{q}_k + \mathbf{G}_d \mathbf{C}^T \lambda \tag{32}$$

Where $\mathbf{G}_d$ is the residual-flexibility matrix. If rigid-body modes exist, the first term of the sum is non-zero and the residual-flexibility matrix must also be inertia-relief.

Subcomponents (1) and (2) can then be both reduced and assembled using the transformation matrix $\mathbf{T}_{\mathbf{DCB}}$ defined in Eq. (33).

$$\left\{\begin{array}{c}\mathbf{x}^{(1)}\\\hline\mathbf{x}^{(2)}\\\hline\lambda\end{array}\right\}=\left[\begin{array}{cc|cc|c}\boldsymbol{\Psi}_r^{(1)}&\boldsymbol{\Phi}_k^{(1)}&0&0&\mathbf{G}_d^{(1)}\mathbf{C}^{(1)T}\\0&0&\boldsymbol{\Psi}_r^{(2)}&\boldsymbol{\Phi}_k^{(2)}&\mathbf{G}_d^{(2)}\mathbf{C}^{(2)T}\\0&0&0&0&\mathbf{I}\end{array}\right]\left\{\begin{array}{c}\mathbf{q}_r^{(1)}\\\mathbf{q}_k^{(1)}\\\hline\mathbf{q}_r^{(2)}\\\mathbf{q}_k^{(2)}\\\hline\lambda\end{array}\right\}=\mathbf{T}_{\mathbf{DCB}}\left\{\begin{array}{c}\mathbf{q}_r^{(1)}\\\mathbf{q}_k^{(1)}\\\hline\mathbf{q}_r^{(2)}\\\mathbf{q}_k^{(2)}\\\hline\lambda\end{array}\right\} \tag{33}$$

$$\tilde{\mathbf{M}}_{\mathbf{DCB}}=\mathbf{T}_{\mathbf{DCB}}^T\left[\begin{array}{ccc}\mathbf{M}^{(1)}&0&0\\0&\mathbf{M}^{(2)}&0\\0&0&0\end{array}\right]\mathbf{T}_{\mathbf{DCB}} \tag{34}$$

$$\tilde{\mathbf{K}}_{\mathbf{DCB}}=\mathbf{T}_{\mathbf{DCB}}^T\left[\begin{array}{ccc}\mathbf{K}^{(1)}&0&-\mathbf{C}^{(1)T}\\0&\mathbf{K}^{(2)}&-\mathbf{C}^{(2)T}\\-\mathbf{C}^{(1)}&-\mathbf{C}^{(2)}&0\end{array}\right]\mathbf{T}_{\mathbf{DCB}} \tag{35}$$

The obtained mass and stiffness matrices using the dual Craig-Bampton method have the advantage of keeping mostly their sparsity unlike the Craig-Chang reduction. Degrees of freedom corresponding to interconnecting forces are added to the final reduced system.

3 SIMPLE BEAM SYSTEM

3.1 Substructuring Example

To demonstrate this theory, the simple beam system from [6] will be used. The schematic of the system is shown in Fig. 2. The red beam is the substructure that we do not want to model analytically. The thick dark red beam, denoted as the TS beam, is the transmission simulator, chosen to mimic the increased stiffness that the red beam will experience when coupled. The red beam with the transmission simulator attached, denoted as the experimental beam, is the substructure of interest, on which we take experimental data. Specifically, the red beam is 15 elements long and the transmission simulator is four elements long which overlaps the left most four elements of the red beam. The blue beam is the finite element model which is 20 elements long, denoted as the FE beam. The plus/cross on the FE beam and the experimental beam are where the two beams overlap and are connected after coupled.

During the substructuring process, the red beam will be coupled to the FE beam to produce the response of two beams attached one the other, denoted as the final system beam. The substructured beam will be compared to the finite element model of the final system beam which acts as the truth model.

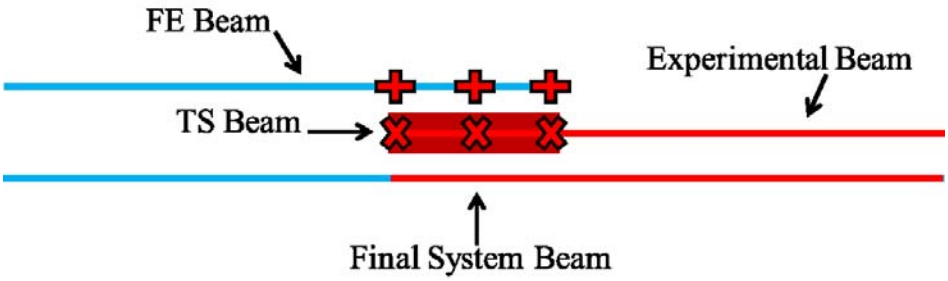

Figure 2: Beam Substructures and Final Assembled Beam

In order to be coupled to the FE beam, the experimental-analytical model of the red beam will be obtained by five substructuring methods which are, in turn, the traditional Transmission Simulator method (TS), the Craig-Mayes method (CM), the Craig-Chang method (CC), the dual Craig-Bampton method (DCB), and finally the Craig-Bampton method (CB).

While it is advantageous to utilize a transmission simulator to mass-load the interface and improve the modal base of the subsystem by the TS and CM method, it is not feasible or even not possible to measure necessary experimental data at the interface by the other traditional substructuring methods, including the CC, DCB, and CB method. As explained in Sec. 2, it requires more involved measurements necessary to obtain the residual flexibility at the interface for the CC and DCB model, and it is not possible to obtain the fixed-interface modes of the CB model experimentally. Therefore, the CC and DCB method are meant to present as other experimentally-based methods, and the CB method is to present simply as an analytical exercise to show how well these experimentally-based methods work compared to the common CB method in FEA.

The substructuring process is summarized in below. First of all, the experimental-analytical model of the red beam was obtained by the aforementioned five methods, respectively. Based on the theory, these five methods obtained the model in different ways. The TS and CM method utilized the transmission simulator to obtain the model and thus were applied to the experimental beam which subtracted the thick dark red beam during the substructuring process. On the other hand, the traditional substructuring methods, including the CC, DCB, and CB method, were directly applied to the red beam and thus did not remove the transmission simulator. Therefore, the modes retained were not identical in each method. For the TS and CM method, all the rigid body modes and the first bending modes of the transmission simulator, and the three rigid body modes and the first seven bending modes (up to 22185.9 Hz) of the *experimental beam* were retained in the formulation. The transmission simulator had six measured degrees of freedom, three vertical translations and three horizontal translations at the three nodes located at the transmission simulator left end, center, and right end, marked by the cross symbols in Fig. 2. For the other methods, all the rigid body modes and the first seven bending modes of the *red beam* (up to 22366.0 Hz) were instead retained. Furthermore, the interface degrees of freedom of the red beam were chosen the same with those of the transmission simulator. Second of all, The experimental-analytical models were individually coupled to the full finite element model of the FE beam via the connection points marked by the plus symbols in Fig. 2. Typically, inclusion of finite element modes is not as limited as experimental modes, and therefore the finite element model of the FE beam was not reduced, retaining all the degrees of freedoms.

To evaluate the methods, the natural frequencies predicted by substructuring are compared for the first ten bending modes (up to 10137.6 Hz) of the truth model. The results of comparison are listed in Table 1 and the relative errors in frequency are listed in Table 2. As shown in Tables 1 and 2, the TS and CM method yielded almost identical natural frequencies and relative errors. On the other hand, the CC and DCB method had almost identical results. Finally, all the experimentally-based methods show satisfactorily converge to the truth frequency within 2% error and to the CB method.

As a final remark, these five methods generated different numbers of spurious modes within the frequency range of interest (the spurious modes were previously filtered out and are not shown in Tables 1 and 2 to save space) in spite of the fact that similar results were obtained in similar methods. The TS and CM method generated fewest spurious modes (two spurious modes of each), followed by the CB and DCB method (three of each), and finally the CC method (four).

TABLE 1: Comparison of beam truth frequency and TS, CM, CC, DCB, and CB substructured frequency (bending modes only)

Truth frequency (Hz)	Frequency TS (Hz)	Frequency CM (Hz)	Frequency CC (Hz)	Frequency DCB (Hz)	Frequency CB (Hz)
211.9	211.2	211.3	208.7	208.7	208.7
574.6	578.6	578.6	571.2	571.2	571.2
1121.0	1114.8	1114.7	1114.1	1114.1	1114.1
1867.3	1869.1	1869.3	1853.4	1853.4	1853.5
2750.2	2741.6	2741.4	2732.1	2731.0	2731.0
3949.6	3949.8	3949.8	3938.5	3938.5	3939.0
5115.9	5104.5	5104.3	5072.9	5073.0	5079.4
6703.0	6710.3	6710.1	6685.4	6685.5	6700.6
8338.9	8311.0	8311.0	8305.6	8305.7	8309.9
10137.6	10150.6	10150.4	10078.6	10080.0	10177.7

3.2 Condition of substructuring

As far as the TS and CM method are concerned, the convergence of substructuring depends on how well-conditioned and accurately the connection point motion can be estimated from the motion at the measurement points. Based on the theory, the

TABLE 2: Relative errors between the truth frequency and TS, CM, CC, DCB, and CB substructured frequency of the beam system (bending modes only)

Relative error TS (Hz)	Relative error CM (Hz)	Relative error CC (Hz)	Relative error DCB (Hz)	Relative error CB (Hz)
-0.35	-0.30	-1.51	-1.51	-1.51
0.70	0.71	-0.60	-0.60	-0.60
-0.56	-0.56	-0.62	-0.62	-0.62
0.10	0.11	-0.74	-0.74	-0.74
-0.31	-0.32	-0.70	-0.70	-0.66
0.01	0.01	-0.28	-0.28	-0.27
-0.22	-0.23	-0.84	-0.84	-0.71
0.11	0.11	-0.26	-0.26	-0.04
-0.33	-0.33	-0.40	-0.40	-0.35
0.13	0.13	-0.58	-0.57	0.40

TS method uses the transmission simulator mode shape matrix $\mathbf{\Phi}_A$ in Eq. (3) to estimate the connection point motion whereas the CM method uses $\mathbf{\Phi}_b^\dagger \mathbf{\Psi}_b$ in Eq. (21). The connection point motion is expanded in the modal spaces spanned by these matrices which have to be full rank. Therefore, the condition numbers of these matrices indicate the condition of substructuring as pointed out in references[1] and [5].

To demonstrate this idea, the influence of the condition numbers of $\mathbf{\Phi}_A$ and $\mathbf{\Phi}_b^\dagger \mathbf{\Psi}_b$ on the simple beam system was examined. Table 3 shows the condition number of $\mathbf{\Phi}_A$ with respect to the number of the transmission simulator modes from the simple beam system. Typically, the measured points are at least as many as there are transmission simulator modes retained. Therefore, Table 3 only shows the condition numbers up to the sixth of the transmission simulator modes. As shown in Table 3, the condition numbers were less than 2.4 when the number of transmission simulator modes was kept less than five. When the number of transmission simulator modes was equal to six the condition number sky-rocketed to 1.14×10^{15}. It was also found that the former yielded the satisfactory convergence of frequency within 0.7% absolute error compared with the truth frequency in Table 1 while the latter yielded one negative frequency and huge errors within the frequency range of interest and the substructuring failed.

TABLE 3: Condition number of $\mathbf{\Phi}_A$ with respect to transmission simulator modes

Number of TS modes retained	Condition number of Φ_A
1	1.00
2	1.17
3	1.41
4	2.31
5	2.31
6	1.14×10^{15}

On the other hand, the condition number of $\mathbf{\Phi}_b^\dagger \mathbf{\Psi}_b$ indicates the condition of substructuring using the CM method. Contrary to the TS method, the condition number of $\mathbf{\Phi}_b^\dagger \mathbf{\Psi}_b$ not only depends on transmission simulator modes but also modes of experimental structure. As a result, a contour plot of the condition number of $\mathbf{\Phi}_b^\dagger \mathbf{\Psi}_b$ with respect to various combination of modes between the transmission simulator and the experimental beam from the simple beam system is plotted in Fig. 3. Totally, 13 modes of the experimental beam were considered which have highest frequency equal to that in Section 3, and again the same six transmission simulator modes were considered. As shown in Fig. 3, when the number of the transmission simulator modes was kept less than four, all the combinations of modes gave relative small condition numbers, shown as the cold region. It was also confirmed that the combinations of modes made in the cold region all led to successful convergence without any spurious mode. When number of the transmission simulator modes was five or six, however, there were some combinations that forbid successful convergence due to large condition numbers (minimum magnitude of 10^{13}), shown as the hot region. Based on the formulation of CM method, the number of modes of experimental structure has be to greater than that of transmission simulator. As such,

when the transmission simulator modes were kept six, all combination of modes were in the hot region. When there were five of the transmission simulator modes, the combination with six or nine of the experimental beam modes were within the hot region. It was found that combinations made in the hot region yielded negative frequencies and led to failure of substructuring.

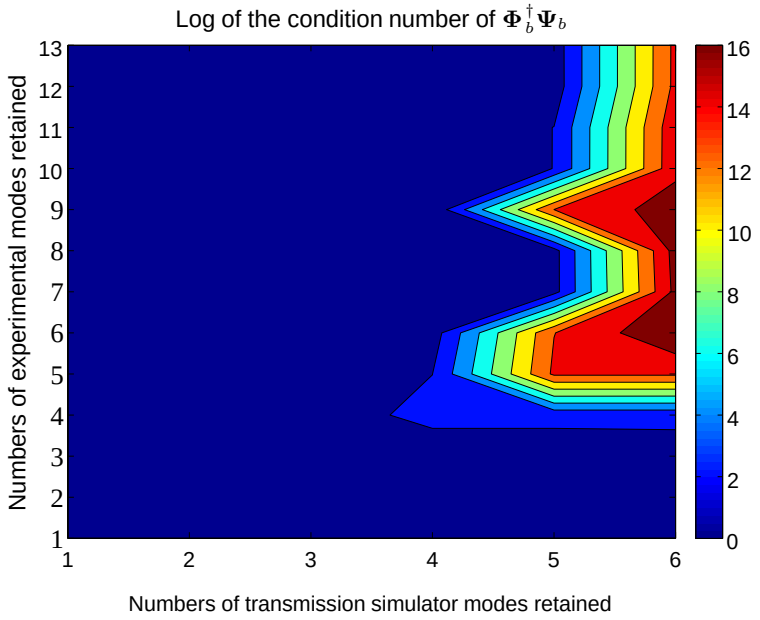

Figure 3: Condition number of $\mathbf{\Phi}_b^\dagger \mathbf{\Psi}_b$ in contour plot

If both $\mathbf{\Phi}_A$ and $\mathbf{\Phi}_b^\dagger \mathbf{\Psi}_b$ are well-conditioned, the TS and CM method show no significant difference. Furthermore, the converge rates were observed improved if the connection point motion were more accurately estimated. Figure 4 shows a convergence study done by using the TS and CM method on the simple beam system with increasing numbers of the experimental beam modes and two different choices of the transmission simulator modes to retain. Consequently, two groups of data sets are presented in Fig. 4. The first group of data concerns the convergence rates of the TS and CM method with retaining only the rigid body modes of the transmission simulator. The second group, on the other hand, considers the convergence rates with additional inclusion of the first bending mode of the transmission simulator. As shown in Fig. 4, after including sufficient (e.g., > 6 for the fist group or > 8 for the second group) experimental beam modes convergence rates had no significant improvement. Further improvement was observed when the first bending mode of the transmission simulator was included. This could be an important point. Including that mode not only gives a better model for the TS, it allows us to more accurately estimate the motion of the connection point, to which the analytical structure will eventually be coupled.

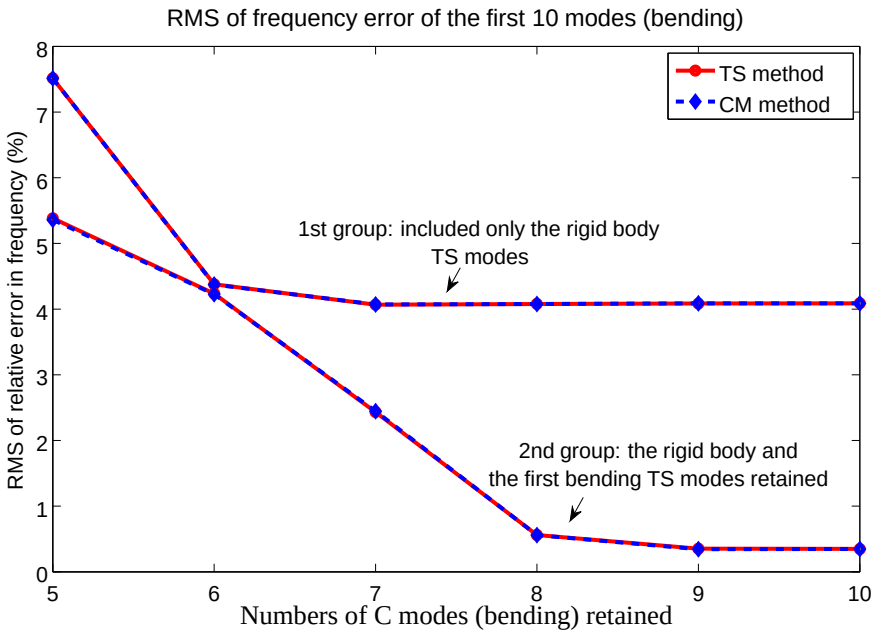

Figure 4: Root mean square (RMS) of relative error in frequency. Comparison with the first ten modes (bending) of the truth model

4 CYLINDER-PLATE-BEAM SYSTEM

4.1 Introduce system

To test this theory with experimental data, a sample experimental system was chosen from [6]. The cylinder-plate-beam (CPB) system consists of a cylinder packed with pressed foam that houses an internal mass. At one end of the cylinder a plate and beam are attached to the system to simulate the rest of the structure of interest. The cross section of a solid model is shown in Fig.5. The cylinder and plate-beam are 6061 T6 aluminum. The goal of this example is to estimate a model for the dynamics of the foam and the internal mass. These internals are extremely challenging to model because the foam's properties are poorly defined and depend non-linearly on the preload in the foam. In addition the contact conditions between the foam and the rest of the structure are not known.

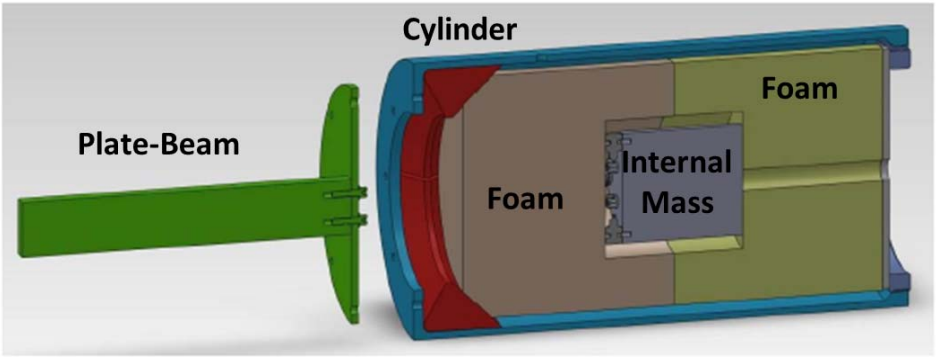

Figure 5: Experimental system solid model

For this, the full CPB system is considered subsystem **C** and will be tested to deduce a model for the internals. The transmission simulator and Craig-Mayes methods can easily be applied using a finite element model of the transmission simulator **A** (consisting of the beam, plate and cylinder) leaving an experimental model for the foam and internal mass. To validate the model for the internals, the authors have added a new beam, plate, and cylinder external system but with a mass loading the end of the beam. This simulates a situation in which the substructure model would be used to predict the response after the other substructures have been modified. A validation test was completed to check the accuracy of the substructuring predictions. Figure6 shows the different subsystems being used in this substructuring example.

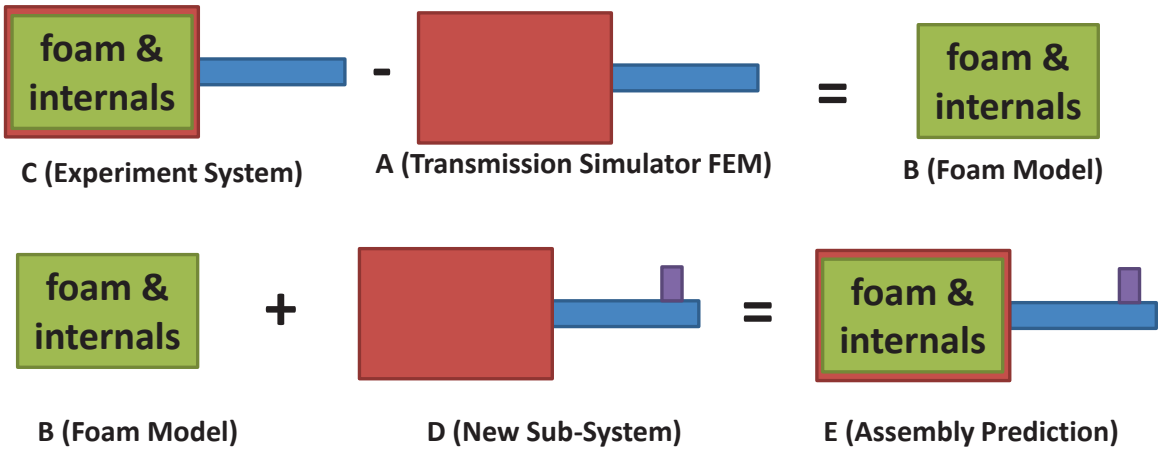

Figure 6: Transmission simulator subsystem designation

4.1.1 EXPERIMENT

A modal test was completed for both the CPB system and the mass-loaded truth test. The system was instrumented with 18 triaxial accelerometers with sensitivities of 100 mV/g. 15 of these accelerometers were placed on the external side of the hardware (12 on the can at three axial stations with four equally spaced around the circumference at each station and 3 on the beam). The remaining 3 triaxial accelerometers were placed on the internal mass, which is packed between the foam blocks. Figure 7 shows the experimental set up for the CPB system with and without the added mass.

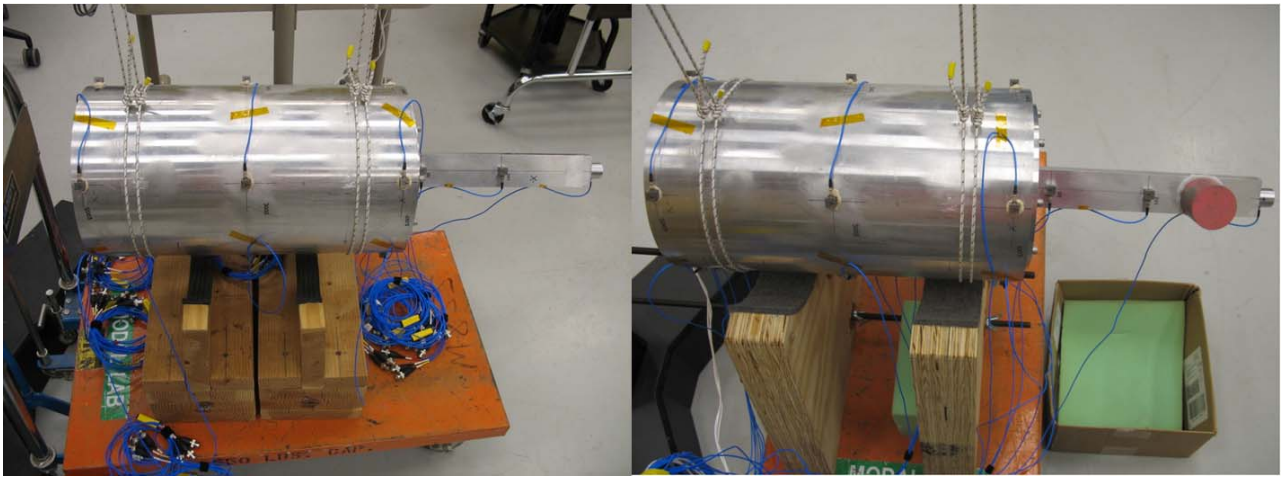

Figure 7: Experimental setup for system C (left) validation test on system E with added mass (right)

The external accelerometers were configured as shown in Fig.8. These were placed to capture the motion of the CPB system up to 1000 Hertz based on previous experience [7].

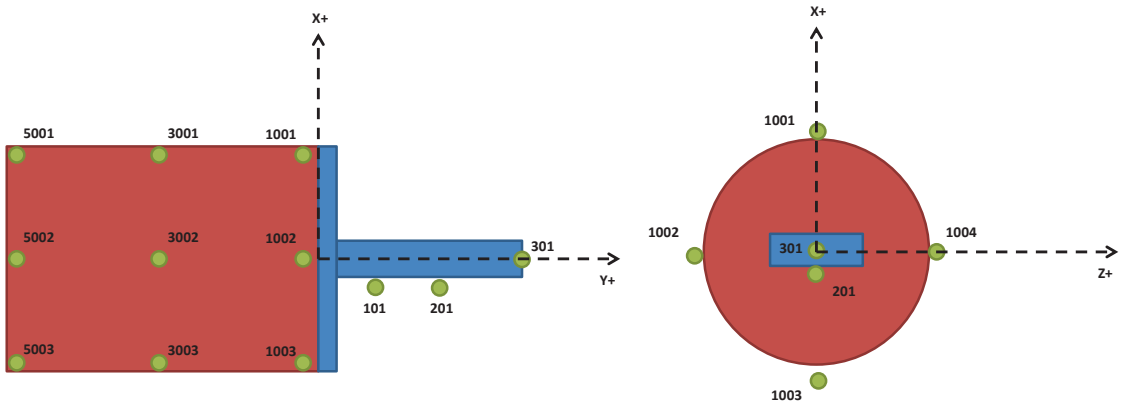

Figure 8: External instrumentation

A series of low-level forcing tests were completed at several driving point locations in order to avoid any non-linearities in the system. For each mode, the location at which it responded most strongly was used to extract the modal parameters using the SMAC algorithm [7]. These driving points are listed in 4 in the column labelled ”Reference”. The information from the linear test on the baseline CPB system is shown in Table 4. Note, the rigid body modes were generated analytically but were checked and compared frequency response function mass-lines.

TABLE 4: Cylinder-plate-beam test results

Mode	Frequency (Hz)	Damping Ratio (%)	Reference	Description
1	1	1	NA	Rigid translation in X
2	1	1	NA	Rigid translation in Y
3	1	1	NA	Rigid translation in Z
4	1	1	NA	Rigid rotation about X
5	1	1	NA	Rigid rotation about Y
6	1	1	NA	Rigid rotation about Z
7	116	0.27	5003X+	1st bending in the X-Direction
8	153	0.15	5002Z+	1st bending in the Z-Direction
9	276	2.37	5002Z+	Internals rotation about Y plus translation in Z
10	282	2.08	5003X+	Internals translation in X and Z
11	300	2.26	5002Z+	Off-axis rotation of internals about Y plus translation in X
12	455	0.32	301Y-	Axial mode, internals and nose out of phase
13	589	2.09	301Y-	Internals rotation about Z
14	634	1.96	5002Z+	Internals rotation about X
15	691	1.28	301Y-	Axial mode, internals and nose in phase
16	742	1.19	3003X+	Suspected foam mode mostly in X
17	761	1.13	3002Z+	Suspected foam mode mostly in Z
18	831	1.00	5002X+	1st Axial Torsion
19	914	0.79	3002Z+	(2,0) ovaling on-axis
20	964	0.22	1301X+	2nd bending in the X-Direction

4.1.2 MODEL

A finite element model (FEM) of the cylinder-plate-beam (CPB) was constructed and is detailed in Fig. 9. The three-dimensional solid structure was modeled by brick type higher order 20-nodes solid elements which exhibits quadratic displacement behavior. The CPB FE model comprises beam, plate, washer, cylinder and ring Fig.9. The FE model was constructed as a single linear structure by merging the adjacent nodes at the contact points between each component. The element properties of all of the components except the washers are set as 6061 T6 Aluminum, with the material properties listed in Table 5. The detailed component name and properties are shown in Table 5. Fifteen nodes were selected as the sensor positions and the mesh was constructed such that these corresponded precisely to the actual accelerometer locations.

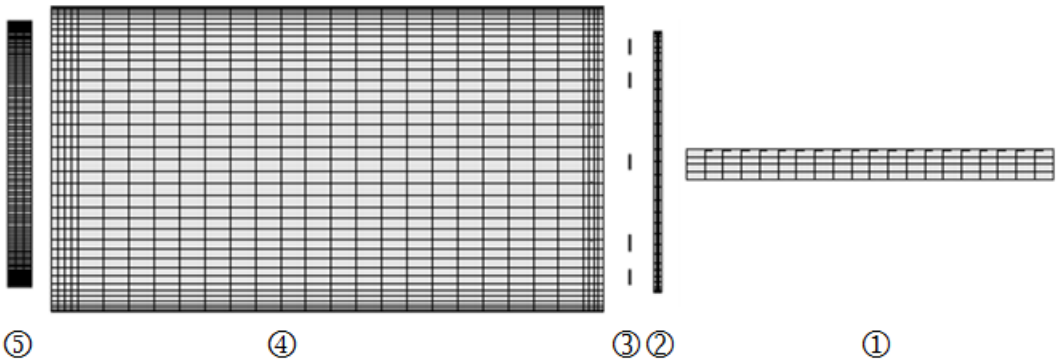

Figure 9: Configuration of CBP FE model: 1 - Beam, 2 - Plate, 3 - Washer, 4 - Cylinder, 5 - Ring

To validate the FE model, the natural frequencies of the cylinder-plate-baem system were examined. Table 6 shows the first eleven elastic frequencies of CPB model with the retaining ring on the far left removed. These are compared to the measured natural frequencies of the actual hardware, from a test that was performed before the foam and retaining ring had been installed. [6]

The additional mass attached at the end of the beam is modeled with 20 node hex elements. The nodes in this mesh did not naturally align with those in the beam mesh, so the two substructures were connected using the multi-point constraint method.

TABLE 5: Element properties of each component

	Component	Material	Material properties
①	Beam	6061 T6 Aluminum	$E = 1.0 \times 10^7,\ \nu = 0.33,\ \rho = 7.126 \times 10^{-4}$
②	Plate	6061 T6 Aluminum	$E = 1.0 \times 10^7,\ \nu = 0.33,\ \rho = 7.126 \times 10^{-4}$
③	Washer	Steel	$E = 3.0 \times 10^7,\ \nu = 0.29,\ \rho = 7.7 \times 10^{-4}$
④	Cylinder	6061 T6 Aluminum	$E = 1.0 \times 10^7,\ \nu = 0.33,\ \rho = 7.126 \times 10^{-4}$
⑤	Ring	6061 T6 Aluminum	$E = 1.0 \times 10^7,\ \nu = 0.33,\ \rho = 7.126 \times 10^{-4}$

TABLE 6: Elastic modal frequencies of CPB

Mode	Test frequency (Hz)	FEM frequency (Hz)	Error(%)
1	134.2	133.83	-0.28
2	171.2	171.30	0.06
3	430	435.15	1.20
4	511.2	497.42	-2.70
5	975.7	954.60	-2.16
6	1027	1038.14	1.08
7	1312	1301.33	-0.81
8	1528	1535.62	0.5
9	1637	1589.17	-2.92
10	1801	1846.45	2.52
11	1833	1859.75	1.46

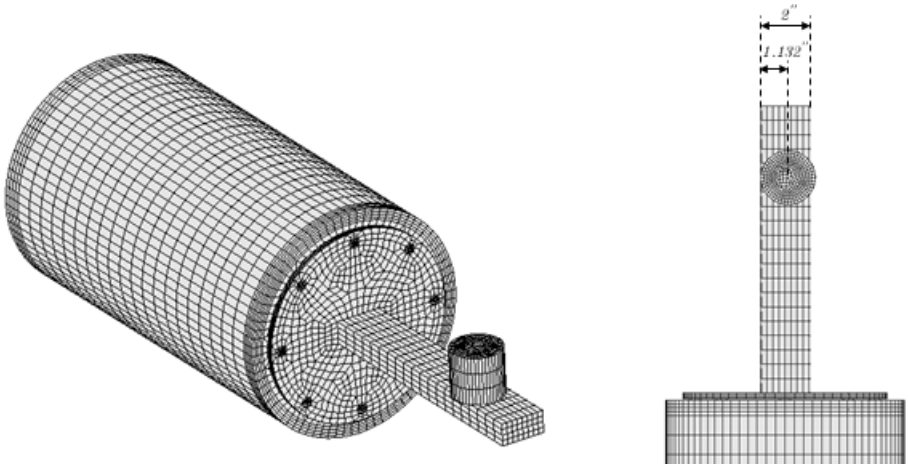

Figure 10: CPB model with additional mass

4.2 Predictions and Comparison with Experimental Truth Data

Here we shall consider a substructuring problem in which the first 20 free normal modes (six rigid body modes and 14 elastic modes) up to 970 Hz were extracted from the experimental system C in Fig.6, consisting of the CBP structure with the foam inside. These 20 free normal modes also included the experimental damping ratio. A FE model of the transmission simulator, i.e. the CBP structure (A in Fig.6), was used to remove the effects of the transmission simulator. From the FE model of the transmission simulator, ten free normal modes (six rigid body modes and the first four elastic modes) up to 805 Hz were retained with an arbitrarily assigned damping ratio of 0.5 percent. Subsequently, the dynamics of the modified CBP structure (i.e. with the mass attached, system D in Fig.6) were added to predict the dynamical behavior of the truth hardware (system E in Fig.6) and shown on the right in Fig.7. The predictions will then be compared to the results of the test on the truth hardware to evaluate the substructuring methods.

Two different substructuring approaches were applied, the traditional transmission simulator method (TS) and the Craig-Mayes

method (CM).

4.2.1 TRADITIONAL TS METHOD

From the FE model of the modified CBP structure D, 13 free normal modes (six rigid body modes and the first seven elastic modes) up to 858 Hz were retained and an arbitrary damping ratio of 0.5 percent was assigned. All three structures (experimental system C, transmission simulator A and modified CBP structure D) were connected using modal constraints at the 45 exterior measurement degrees of freedom (i.e. $\Phi_A^\dagger$ in Eq. (4) contained 45 rows corresponding to all of the exterior measurement degrees of freedom).

Table 7 shows the prediction obtained by the traditional TS method compared to the truth experiment E.

Traditional Transmission Simulator method							
Mode No.	$f_{experiment}$	$f_{prediction}$	f error	$\zeta_{experiment}$	$\zeta_{prediction}$	ζ error	MAC
[-]	[Hz]	[Hz]	[%]	[-]	[-]	[%]	[-]
7	88.33	86.59	-1.96	0.00196	0.00215	9.38	0.9803
8	115.80	115.06	-0.64	0.00163	0.00207	26.83	0.9929
9	275.97	276.11	0.05	0.02468	0.02466	-0.10	0.9006
10	283.32	283.24	-0.03	0.02151	0.02168	0.80	0.9995
11	301.40	301.77	0.12	0.02327	0.02290	-1.61	0.9957
12	346.25	349.76	1.01	0.00291	0.00359	23.47	0.9867
13	584.71	583.20	-0.26	0.02119	0.02135	-0.77	0.9963
14	635.16	634.89	-0.04	0.02037	0.01897	-6.87	0.9948
-	NA	670.72	NA	NA	0.00504	NA	NA
15	688.92	690.36	0.21	0.01515	0.01363	-10.03	0.9320
-	NA	717.45	NA	NA	0.00537	NA	NA
16	758.36	NA	NA	0.01131	NA	NA	NA
17	769.71	770.99	0.17	0.01191	0.01201	0.84	0.8827

TABLE 7: Frequencies, damping ratios and MAC values, Traditional Transmission Simulator method

The modes are well predicted up to the 14th mode at 635 Hz, with relative frequency errors between -1.96 % and 1.01 %, relative damping errors between -6.87 % and 26.83 % and MAC values between 0.9006 and 0.9995.

By visualizing the predicted mode shapes with a wireframe model built of the sensor nodes, the modes predicted at 670.72 Hz and at 717.45 Hz could be identified as non-physical, so-called spurious modes. In this case, the traditional TS Method is not able to predict the 16th mode of the truth experiment at 758.36 Hz with the number of modes retained from the transmission simulator and from the modified CBP structure.

In figure 11, the MAC values for the mode shapes predicted by the traditional TS method and the true experimental mode shapes are shown.

4.2.2 CRAIG-MAYES METHOD

The FE model of the modified CBP structure D was transformed to Craig-Bampton coordinates after arbitrarily assigning a damping ratio of 0.5 percent. Eight fixed-interface normal modes up to 1898 Hz were retained during the transformation. Here, the 45 exterior measurement degrees of freedom were considered as the interface and held fixed. The Craig-Mayes representation resulting from the experimental system C and the transmission simulator A was connected to the Craig-Bampton representation of the modified CBP structure D by primal assembly at the 45 exterior measurement degrees of freedom.

Table 8 shows the prediction obtained by the Craig-Mayes method compared to the truth experiment E.

The modes are well predicted up to the 14th mode at 635 Hz, with the relative frequency errors ranging from -0.47 % to 1.42 %, relative damping errors between -6.69 % and 25.14 % and the MAC values ranging from 0.8886 to 0.9986.

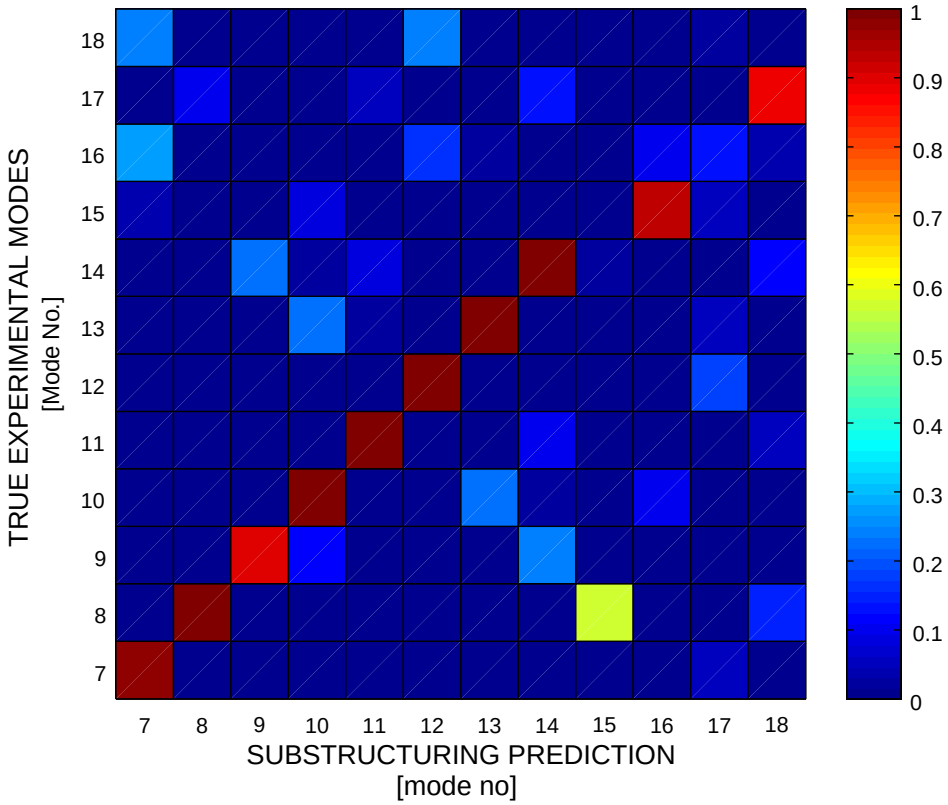

Figure 11: MAC traditional TS method vs. Truth

Craig-Mayes Transmission Simulator method							
Mode No.	$f_{experiment}$	$f_{prediction}$	f error	$\zeta_{experiment}$	$\zeta_{prediction}$	ζ error	MAC
[-]	[Hz]	[Hz]	[%]	[-]	[-]	[%]	[-]
7	88.33	89.58	1.42	0.00196	0.00208	5.84	0.9861
8	115.80	115.25	-0.47	0.00163	0.00204	25.14	0.9975
9	275.97	275.83	-0.05	0.02468	0.02459	-0.36	0.8886
10	283.32	282.61	-0.25	0.02151	0.02156	0.23	0.9986
11	301.40	301.48	0.03	0.02327	0.02284	-1.84	0.9966
12	346.25	350.61	1.26	0.00291	0.00343	17.96	0.9897
13	584.71	583.64	-0.18	0.02119	0.02141	1.05	0.9971
14	635.16	634.85	-0.05	0.02037	0.01900	-6.69	0.9961
-	NA	679.99	NA	NA	0.00491	NA	NA
15	688.92	691.85	0.43	0.01515	0.01351	10.83	0.9075
-	NA	707.57	NA	NA	0.00574	NA	NA
16	758.36	NA	NA	0.01131	NA	NA	NA
17	769.71	760.69	-1.17	0.01191	0.01125	-5.54	0.8308

TABLE 8: Frequencies, damping ratios and MAC values, Craig-Mayes method

The modes predicted at 679.99 Hz and at 707.57 Hz could be identified as spurious modes. Here, the Craig-Mayes method is not able to predict the 16th mode of the truth experiment at 758.36 Hz with the number of modes retained from the transmission simulator and from the modified CBP structure.

In figure 12, the MAC values for the mode shapes predicted by the Craig-Mayes method and the true experimental mode shapes are shown.

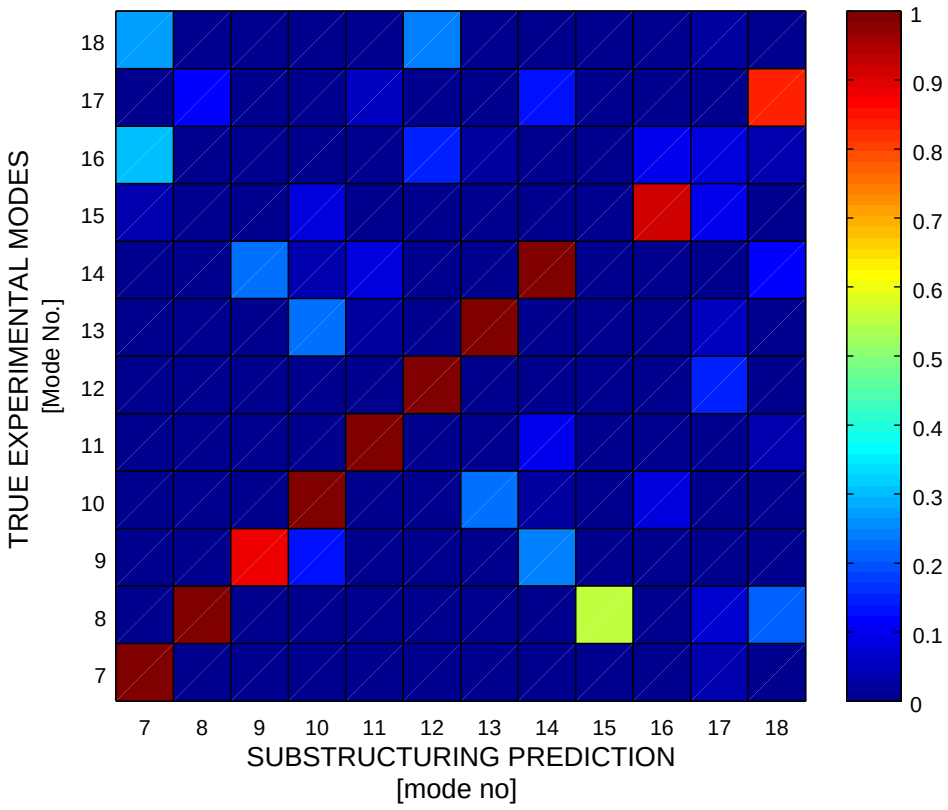

Figure 12: MAC Craig-Mayes method vs. Truth

4.2.3 OBSERVATIONS AND COMPARISON OF TRADITIONAL TS METHOD AND CRAIG-MAYES METHOD

The traditional TS method and the Craig-Mayes method show the same characteristics concerning the number of modes used for the respective substructuring steps and the frequency and damping predictions for system E.

The number of modes used for the subtraction of the transmission simulator (CBP structure A) was varied. With both methods, at least the six rigid body modes plus two elastic modes up to 178 Hz were needed to get results with a relative frequency error smaller than 10 % and a relative damping error smaller than 100 %. As soon as the number of modes used for the subtraction exceeded the frequency range of the experimental system C, the relative frequency errors were bigger than 40 % and no meaningful results could be obtained for the damping using either of the methods.

The number of modes used to add the dynamics of the modified CBP structure D was varied, too. Enough modes to cover the same frequency range as at the subtraction of the TS had to be used in order to get frequency errors smaller than 10 % after the addition of the modified CBP structure (free normal modes for the traditional TS method and fixed-interface normal modes for the Craig-Mayes method). Once that number of modes was reached, using more modes of the modified CBP structure only affected the second decimal place of the frequency predictions and also no significant change in the damping predictions could be observed for either of the methods.

Both methods predict the modes of the truth experiment E up to 635 Hz (mode no 14) quite well, which is more than half of the frequency range considered (970 Hz system C). The relative frequency errors range from -1.96 % to 1.01 % (traditional

Transmission Simulator method) and -1.17 % to 1.42 % (Craig-Mayes method), respectively. The relative damping errors range from -6.87 % to 26.83 % (traditional Transmission Simulator method) and -6.69 % to 25.14 % (Craig-Mayes method), respectively. Regarding those relative frequency and damping errors, the two methods are almost equivalent in their predictions.

The traditional TS method and the Craig-Mayes method both predict a spurious mode between the 14th mode and the 15th mode and between the 15th mode and the 16th mode of the truth system. As applied here, neither of both methods is able to predict the 16th mode of the truth system at 758.36 Hz. In figure 13, the MAC values for the mode shapes predicted by the Craig-Mayes method and the the mode shapes predicted by the traditional TS method are shown. The lowest MAC value on the diagonal is 0.9483 at mode no 17, showing that both methods predict almost the the same mode shapes for the truth system (including the two spurious modes).

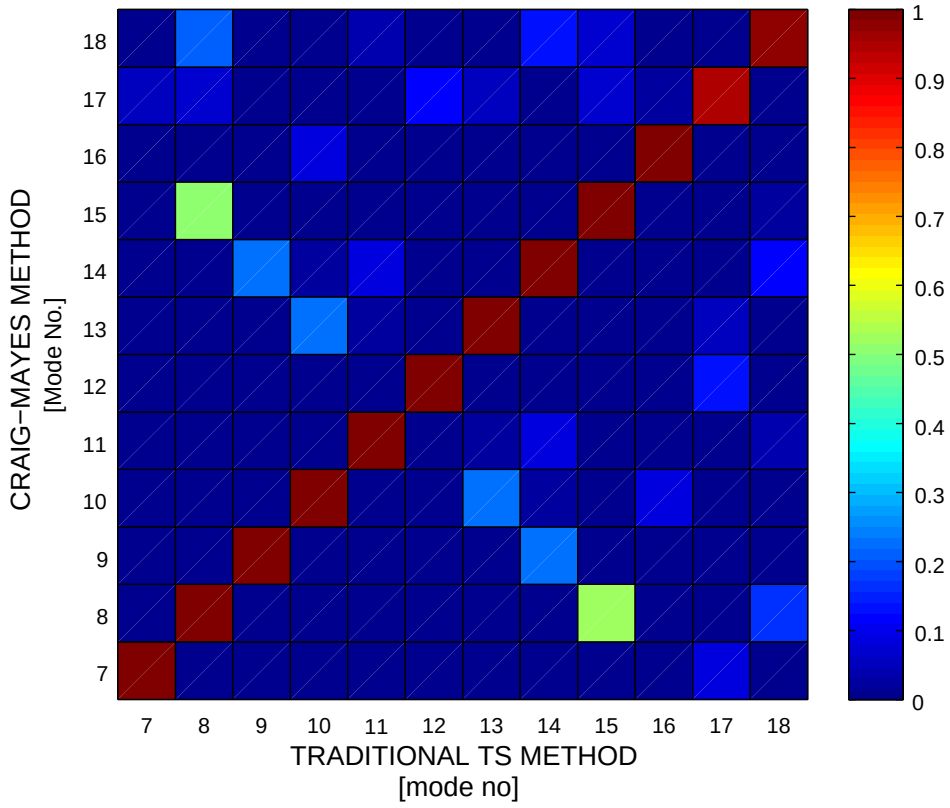

Figure 13: MAC Traditional TS method vs. Craig-Mayes method

The traditional TS method and the Craig-Mayes method both seem to be well suited to predict the frequencies, damping and mode shapes of the modified CBP structure with the foam inside up to half of the frequency range considered.

5 CONCLUSIONS

This paper presented multiple examples of both the Transmission Simulator method and the Craig-Mayes method. The first example was of a simple beam model where the TS and CM methods were compared. Additional comparisons were made to the Craig-Chang, Craig-Bampton, and dual Craig-Bampton methods. In these comparisons the TS and CM methods were found to have similar results with a maximum frequency error of 0.70%. This paper also looks at a few parameters to be checked when completing the TS and CM methods. Of particular note the TS method requires the mode shapes to be well conditions such that the pseudo-inverse performs a quality operation. In contrast, the CM method requires that the mode shapes be well condition when partitioned to just the connection degrees of freedom.

The second example is completed on the Cylinder-Plate-Beam system. In this example, both the TS and CM methods are employed to remove the cylinder-plate-beam from experimental results generating an experimental model of just the internal foam and mass. A finite element model of the cylinder-plate-beam is used as a transmission simulator for both of these methods. Another FEM model with an additional mass added to the beam is then substructured with the experimental foam model. This process was completed with both the traditiona transission simulator and the Craig-Mayes formulation. After comparing these results to an experimental truth test the maximum frequency error was less than 2% while the maximum damping error was near 25% for both methods.

REFERENCES

[1] M. Allen, R. Mayes, and E. Bergman, “Experimental modalsubstructuring to couple and uncouple substructures with flexible fitures and multi-point connections,” *Journal of Sound and Vibration*, vol. 329, pp. 4891–4906, 2010.

[2] R. Mayes, M. Allen, and D. Kammer, “Correcting indefinite mass matrices due to substructure uncoupling,” *Journal of Sound and Vibration*, vol. 332, pp. 5856–5866, 2013.

[3] M. Allen, D. Kammer, and R. Mayes, “Metrics for diagnosing negative mass and stiffness when uncoupling experimental and analytical substructures,” *Journal of Sound and Vibration*, vol. 331, pp. 5435–5448, 2012.

[4] R. Craig and A. Kurdila, *Fundamentals of Structural Dynamics, 2nd ed.* John Wiley & Sons, Inc. Hoboken, New Jersey, 2006.

[5] R. Mayes, “A craig-bampton experimental dynamics substructure using the transmission simulator method,” in *Proceedings of the 33rd International Modal Analysis Conference*, January 2015.

[6] R. Mayes and D. Rohe, “Coupling experimental and analytical substructures with a continuous connection using the transmission simulator method,” in *in 31st International Modal Analysis Conference*, 2013.

[7] D. P. Hensley and R. L. Mayes, “Extending smac to multiple references,” in *Proceedings of the 24th International Modal Analysis Conference*, no. pp 220-230, January 2006.